

# Endofluorescence Imaging of Murine Hepatocellular Carcinoma Cell Culture by Fluorescence Lifetime Microscopy with Modulated CMOS Camera

Elena Potapova<sup>1\*</sup>, Evgeny Zherebtsov<sup>1</sup>, Ksenia Kandurova<sup>1</sup>, Alexander Palalov<sup>1</sup>, Viktor Dremin<sup>1,2</sup>, and Andrey Dunaev<sup>1</sup>

<sup>1</sup> Research and Development Center of Biomedical Photonics, Orel State University, 95 Komsomolskaya str., Orel 302026, Russia

<sup>2</sup> College of Engineering and Physical Sciences, Aston University, Aston Triangle, Birmingham B4 7ET, UK

\* e-mail: [potapova\\_ev\\_ogu@mail.ru](mailto:potapova_ev_ogu@mail.ru)

**Abstract.** In this work, we propose the results of pilot studies on using the modulated CMOS camera for the imaging of autofluorescence in murine hepatocellular carcinoma cells with excitation in UV light. Here, we assess the capabilities of the imaging system to detect changes in the NAD(P)H fractions produced and utilised in the glycolysis, pentose phosphate pathway and oxidative phosphorylation. Our results suggest that the camera and the system based on one possess a sufficient margin of SNR and sensitivity to detect the cellular metabolic changes associated with the metabolic pathways mentioned. © 2022 Journal of Biomedical Photonics & Engineering.

**Keywords:** hepatocellular carcinoma; metabolism; frequency domain fluorescence lifetime imaging.

Paper #3464 received 17 Nov 2021; revised manuscript received 24 Feb 2022; accepted for publication 25 Feb 2022; published online 22 Mar 2022. [doi: 10.18287/JBPE22.08.010303](https://doi.org/10.18287/JBPE22.08.010303).

## 1 Introduction

Liver cancer is characterized by its rapid progression, so the issues of timely diagnosis and further treatment do not lose their relevance [1]. Improvement of medical diagnostic technology and the introduction of new modern methods can help to identify pathological changes at the initial stages and increase the effectiveness of traditional diagnostic procedures [2]. Biophotonics methods can be used to obtain data on the metabolic state of the liver and tumour tissues. In particular, fluorescence methods demonstrate high sensitivity to changes in the metabolic state of tissues. For this reason, the evaluation of the spectral and temporal parameters of fluorescence can serve as a diagnostic criterion, including in oncology [3]. Modern technologies allow combining fluorescent measurements with standard tools for minimally invasive surgery [4–7]. An important step in developing this approach is a fundamental study of the metabolic state of malignant cells to understand their biochemical processes better and correctly interpret the data obtained at the tissue and organ levels.

Uncontrolled tumour growth is accompanied by numerous disorders of redox balance and changes in metabolic pathways, including glycolysis and the pentose

phosphate pathway [8]. The redox states of the NADH and NADPH pools play an important role in determining the activity of energy production paths, in managing oxidative stress and in maintaining antioxidant defence. Because the fluorescence spectra of NADH and NADPH are indistinguishable, interpretation of signals resulting from their combined fluorescence can be challenging [9]. At the same time, measurements of fluorescence intensity may be affected by inhomogeneous surface illumination, the presence of blood and photobleaching. Registering fluorescence lifetime can eliminate these limitations. This technology is sensitive to intermolecular interactions [10] and allows the recognition of endogenous fluorophores with overlapping spectra.

This work aimed to study the imaging of NAD(P)H autofluorescence intensity and lifetime parameters by a setup for fluorescence lifetime microscopy (FLIM) based on a camera with two-tap CMOS sensor for measurements in the frequency domain (pco.flim, PCO GmbH, Germany). The implementation of measurements in the frequency domain with the camera benefits from significantly lower prices for the equipment when compared with the equipment for FLIM imaging in the time domain. Previously, the camera was successfully used for widefield imaging of protoporphyrins in brain

tumours *in vivo* [11]. Nevertheless, the capabilities of the CMOS-based FLIM technique in the frequency domain for the imaging of weak NADH autofluorescence signals from cells require dedicated studies in the aspects of the sufficiency of their signal-to-noise ratio and sensitivity.

In this work, we evaluate NAD(P)H autofluorescence imaging using frequency domain, full-frame FLIM microscopy to identify changes in metabolic activity in the H33 hepatocellular carcinoma cell culture. The results obtained in this work may assist transition of the technique to medical practice to identify characteristic patterns of physiological parameters in hepatocytes and the cells of liver cancer, as well as to identify potential diagnostic criteria to distinguish them.

## 2 Materials and Methods

### 2.1 Experimental setup

The experimental setup (Fig. 1) included a frequency domain CMOS camera pco.flim (PCO AG, Germany) operated at the modulation frequency of 40 MHz and image resolution of 1008×1008 pixels. A 375 nm laser (PCO AG, Germany) was used to excite the autofluorescence in cells. The camera was connected to an inverted biological microscope, IX73 (Olympus Corporation, Japan) with a 40× objective. The exposure time of 500 ms was typically used for the images and results presented in the paper. The output power of the UV laser did not exceed 10 mW before coupling the microscopy system and was at the level of 0.7 mW in the field of view of the objective. The fluorescence lifetimes were estimated by the phase shift and the change in the modulation index of the recorded fluorescence radiation relative to the amplitude-modulated exciting radiation.

### 2.2 Cell culture

A cell culture of murine H33 hepatocellular carcinoma (HCC) was used as the object of study. H33 HCC were established from primary mouse tumours that were induced using a diethylnitrosamine/phenobarbital

protocol and propagated by subcutaneous transfer between mice [12]. The cells were cultured in Dulbecco's modified Eagle medium (DMEM), supplemented with 10% of foetal bovine serum, penicillin and streptomycin, at 37 °C, 100% relative humidity, under an atmosphere containing 5% CO<sub>2</sub> and 95% air. Cells were placed in 35- mm dishes and measured after 3–4 days.

For inducing changes in metabolism in the cell culture of murine H33, well-known pharmacological agents were used, which can simulate various metabolic changes, including influence on redox states of the NADH and NADPH pools. Dehydroepiandrosterone (DHEA), iodoacetic acid (IA), Carbonyl cyanide-4-(trifluoromethoxy)phenylhydrazone (FCCP) and rotenone were all purchased from Sigma-Aldrich. The concentrations of pharmacological agents were chosen by standard or slightly exceeding the concentrations used to alternate metabolism in cultured cells. DHEA is a known non-competitive inhibitor of glucose-6-phosphate dehydrogenase (G6PDH), the rate-limiting step in the pentose phosphate pathway [13]. Iodoacetic acid (IA) is reported as an inhibitor of glycolysis, acting primarily on the enzyme glyceraldehyde-3-phosphate dehydrogenase, which catalyses the conversion of glyceraldehyde-3-phosphate into the high-energy phosphate compound, 1,3 bisphosphoglycerate with the reduction of NAD to NADH [14]. FCCP is a known uncoupling agent of the mitochondrial electron transport chain [15]. FCCP can disrupt ATP synthesis through uncoupling the proton gradient generated by the mitochondrial membrane. Rotenone acts as a strong inhibitor of complex I of the mitochondrial respiratory chain [16].

The measured cells included the control group (N = 9), one treated with iodoacetic acid (20 μM, N = 4) 2 h prior to measurements, and one treated with dehydroepiandrosterone (DHEA, 10 μM, N = 4) 15 min prior to measurements. The measurements included recording of the basal fluorescence signal, fluorescence signal after addition of oxidative phosphorylation uncoupler FCCP (0.2 mM), and complex I inhibitor rotenone (0.02 mM). The measurements lasted for 15 min.

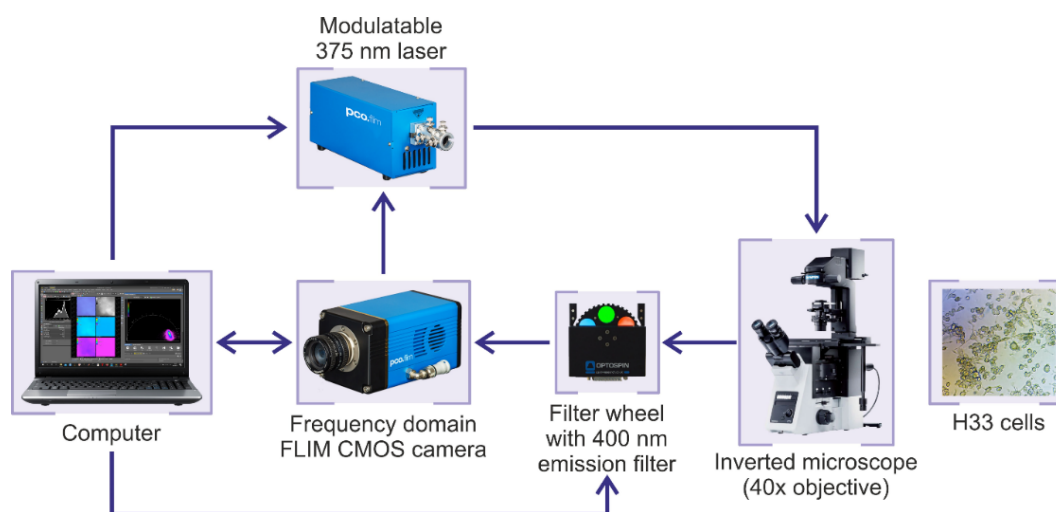


Fig. 1 Schematic diagram of the FLIM setup used for the imaging of H33 cells.

### 2.3 Fluorescence Measurements

Measurement of mitochondrial NADH autofluorescence in live cells was performed according to the algorithm described in Ref. [17]. After stabilizing the autofluorescence signal 1  $\mu$ M FCCP was added to maximize mitochondrial respiration. Waited again to stabilize the autofluorescence signal and was added 1 mM rotenone which blocks the mitochondrial electron transport chain. The total NADH pool value in cells is the difference between the average fluorescence values after application of rotenone and the average fluorescence values after addition of FCCP provides. The averaged maximum fluorescence values obtained after rotenone addition and the averaged minimum fluorescence values obtained after FCCP addition represent 100% and 0% respectively. The values within the 0–100% scale represent the NADH redox index.

In this study, we measured bound and unbound NAD(P)H ratio using the phasor approach to FLIM [18–20]. The autofluorescence emitted in cells after excitation at a wavelength of 375 nm originates from NAD(P)H (free and bound) and FAD. When using an optical filter (400 nm), the fluorescence of NADH can be separated from the FAD contribution. Analysis of fluorescence lifetime in each pixel was carried out following the phasor approach to the FLIM. The phasor coordinates  $G$  and  $S$  in a pixel with coordinates  $i, j$  were calculated in the frequency domain:

$$\begin{aligned} G_{i,j}(\omega) &= m_{i,j} \cos(\varphi_{i,j}), \\ S_{i,j}(\omega) &= m_{i,j} \sin(\varphi_{i,j}), \end{aligned} \quad (1)$$

where  $m_{i,j}$  and  $\varphi_{i,j}$  are the measured modulation index and the phase shift of the emission with respect to the excitation. For each pixel, the lifetimes are calculated based on modulation index ( $\tau_m$ ) and the phase shift ( $\tau_\phi$ ) as follows:

$$\begin{aligned} \tau_\phi &= \omega^{-1} \tan(\phi), \\ \tau_m &= \frac{1}{\omega} \sqrt{\frac{1}{m^2} - 1}. \end{aligned} \quad (2)$$

### 2.4 Statistical Analysis and Images

Fluorescence lifetime parameters and final phasor plots were obtained using NIS-Elements software (Nikon Instruments Inc.). Comparisons between the studied groups were performed using the one-way analysis of variance (ANOVA test). Statistics tests and histograms generation were performed using OriginPro 2015 (OriginLab). Fluorescence intensity images and lifetime maps were processed using ImageJ (National Institutes of Health).

## 3 Results and Discussion

First, the imaging system was calibrated with a fresh 0.1 mM NADH solution. Representative examples of the phasor plot of autofluorescence were obtained from the NADH solution. Representative examples of the phasor plots of autofluorescence obtained from the NADH solution and HCC cells after the calibration procedures are shown in Fig. 2(a) and Fig. 2(b), respectively. The allocation of the points on the universal circle (Fig. 2(a)) suggests the pure single-exponential decay of the measured signal from the NADH solution. The distribution of the data points in images obtained from H33 cells had the shape of an oval inside the universal circle, which points to two-exponential decay in the time domain and the presence of two independent lifetimes in the mix of fluorescence agents in the cells.

Fig. 3 shows the fluorescence intensity (first column) and lifetime maps (colour) of phase shift (second column) and modulation index (third column) of murine H33 cells in the control (first line), IA (second line) and DHEA (third line) experiments.

The analysed parameters included NADH pool, NADH redox index, and phase and modulation indexes characterizing the first and second components of fluorescence lifetime decay (Fig. 4). The statistical significance of the differences was assessed using the one-way ANOVA test ( $p < 0.05$ ).

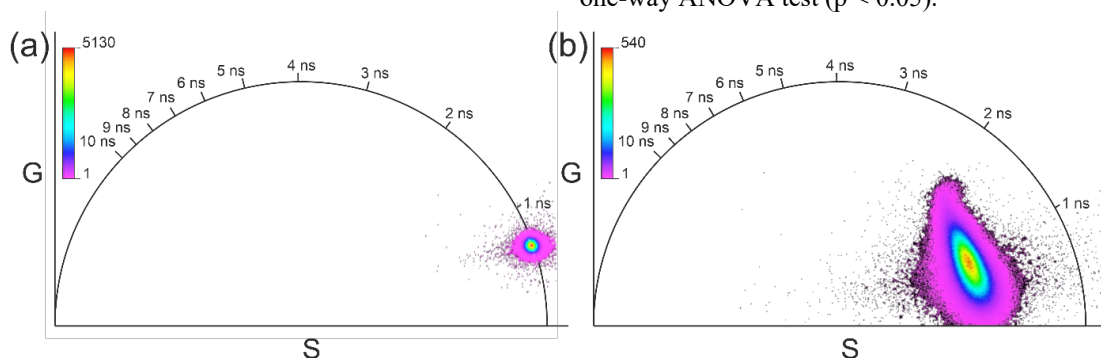


Fig. 2 Representative examples of the phasor plots of autofluorescence obtained from the NADH solution (a) and HCC cells (b).

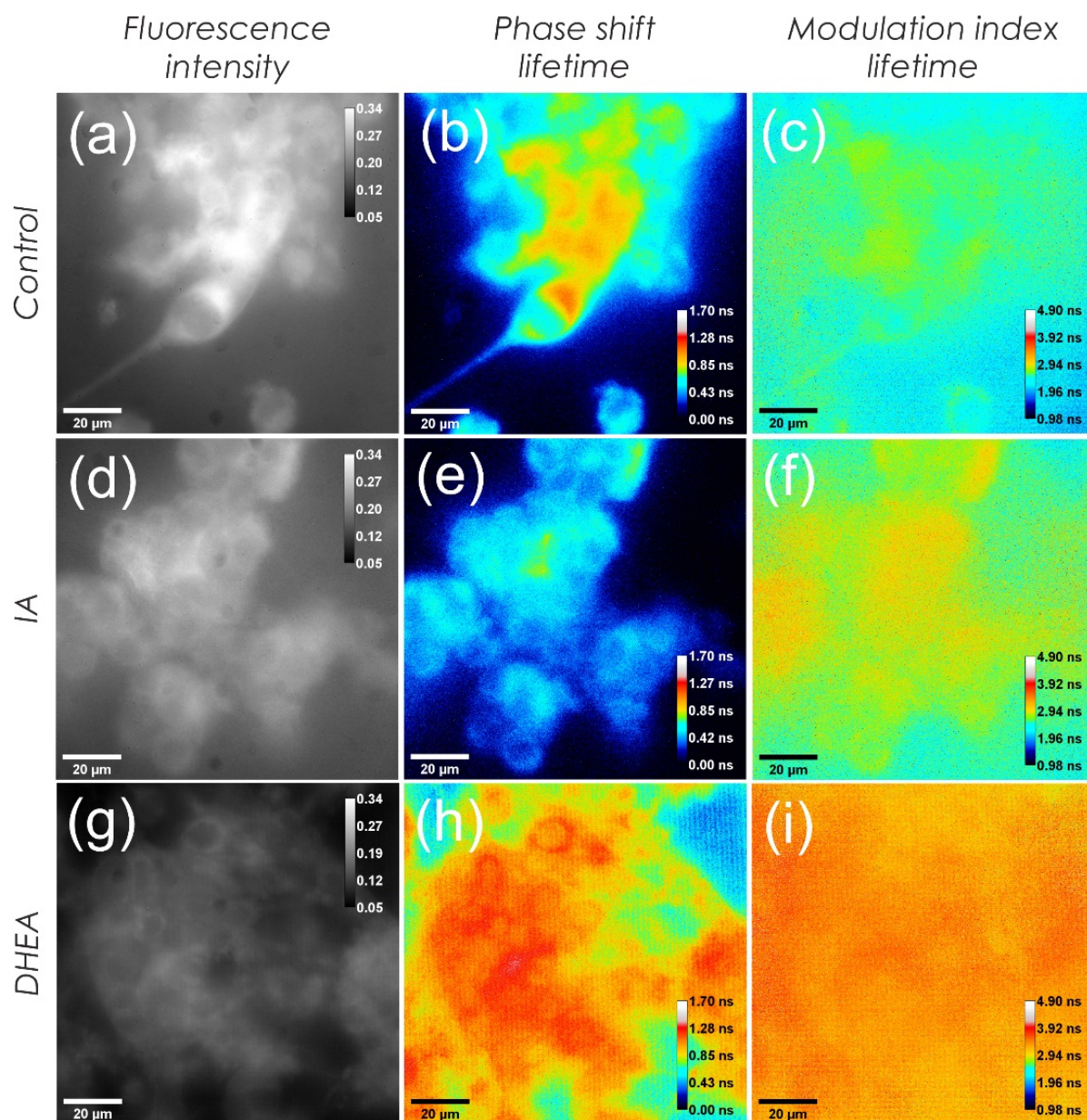


Fig. 3 Fluorescence intensity and lifetime maps (colour) of cells of murine H33 in control (a, b, c), iodoacetic acid (IA) (d, e, f) and dehydroepiandrosterone (DHEA) (g, h, i) experiments.

The results demonstrated a decrease in the average NADH pool, in both IA and DHEA groups ( $41 \pm 27$  a.u.,  $37 \pm 7$  a.u.,  $30 \pm 18$  a.u., respectively), while the NADH redox index increased by more in the IA group ( $53\% \pm 27\%$ ,  $76\% \pm 16\%$ ,  $70\% \pm 17\%$ ). Lower values of the redox index indicate more significant respiratory activity of cells. FCCP was used to uncouple ATP phosphorylation from the electron transport chain, resulting in unregulated, increased oxidation of NADH back to NAD. Uncoupling phosphorylation caused a decrease in the first and second components of the fluorescence lifetime in the control, IA and DHEA experiments. Inhibition of the activity of the electron transport chain by adding rotenone, a blocker of NADH dehydrogenase (complex I), increased the weighted lifetimes of the two components in all experiments. Therefore, it can be concluded that the application of

inhibitors worsened the condition of the cells to different degrees. The observed changes may indicate that liver cancer cells use the process of glycolysis for glucose oxidation and energy production in the form of ATP to a greater extent than the pentose phosphate pathway. Inhibition of glycolysis is more critical for the viability of this cell culture. Inhibition of glycolysis IA led to a significant decrease in the first and second components of fluorescence lifetime decay in basal measurements (53.8% and 7.4%, respectively). In contrast, inhibition of the pentose phosphate pathway using DHEA led to a statistically significant increase in these parameters in the basic test (22.2% and 11.4% respectively). All three groups showed similar dynamics of changes. However, a significant scatter of the obtained values was observed in the control group, which made it difficult to assess in

more detail possible changes in the ratio of bound and unbound NAD(P)H.

In 1979, B. Chance described the idea that NADH autofluorescence can be used as a marker of the redox state of cells and cellular energy metabolism [21]. The intensity of autofluorescence with UV excitation mostly indicates the total amount of NADH. At the same time, NADH has short and long lifetime components, depending on its protein binding status. According to changes in the relative ratio of free and bound NADH, it is possible to estimate the cellular metabolic redox status [22]. In this study, we show that the frequency domain FLIM technique based on the two tap CMOS image sensor can be used as a valuable tool for non-invasive and marker-free study of metabolic changes in living cell cultures *in vitro*. Fluorescence lifetime is specific to molecular species, so the ratio of free/bound

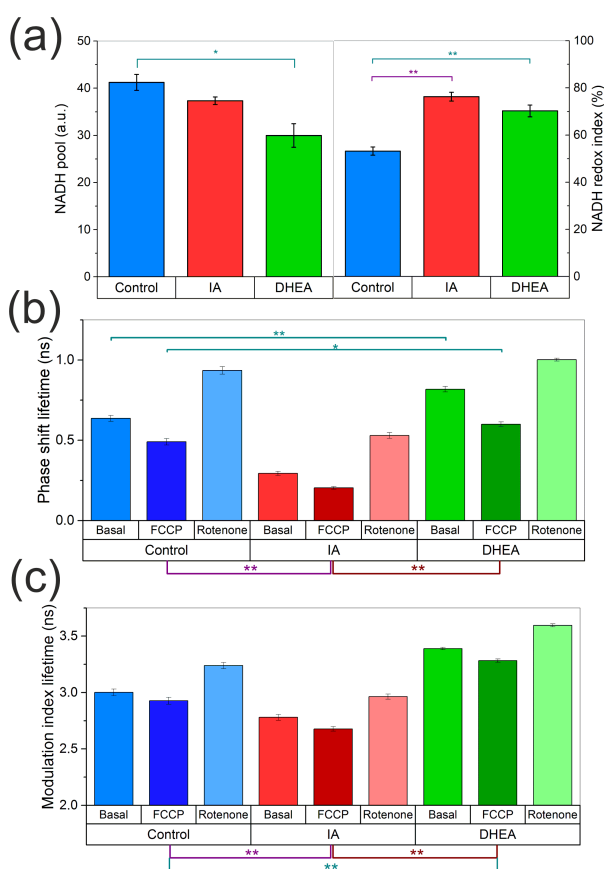


Fig. 4 Computed parameters NADH pool (a-left axis), NADH redox index (a-right axis), and phase shift (b) and modulation index (c) based fluorescence parameters characterizing the first and second components of fluorescence lifetime under varied metabolic conditions (IA – iodoacetic acid, DHEA – dehydroepiandrosterone, FCCP – carbonyl cyanide-4-(trifluoromethoxy) phenylhydrazone). A single SE was taken to plot error bars.

NADH can be measured in each pixel. This is important for expanding the understanding of tumour metabolic mechanisms. Earlier results obtained in the study of liver tumours using multiphoton microscopy FLIM with TCSPC system showed that Time-Domain FLIM can simultaneously display and quantify the cellular morphology and microenvironment of the living liver without fluorescent dyes [23, 24]. The key advantage of frequency-domain FLIM is its fast lifetime image acquisition; moreover, frequency-domain FLIM can be implemented without the use of costly pulsed lasers.

Raman microscopy can also be noted among the methods for studying the metabolic features of tumours [25]. Raman imaging allows one to examine cellular conditions in a non-invasive and non-destructive way. However, it is difficult to quantify metabolic changes in a single cell using only Raman microscopy. Most disadvantages of Raman spectroscopy are related to the weakness of the Raman effect, which leads to longer measurement times and possible damage to cells by thermal heating from the laser. However, it is worth mentioning the promising development of the combined Raman imaging and fluorescence lifetime imaging microscopy systems for diagnosis of cancer state and metabolic monitoring [26] and surface-enhanced Raman scattering (SERS) technique in Raman microscopy [27].

## 4 Conclusion

The obtained data on the application of the new type of frequency domain FLIM camera showed the feasibility of imaging the endogenous fluorescence and fluorescence lifetime parameters to be used for evaluating metabolic processes in cells. The preliminary studies with the imaging system allowed us to observe the criticality of glycolysis for the functioning of malignant cells.

The obtained results of the work and further research can become a scientific basis for the development of diagnostic methods for assessing mitochondrial function in liver tissues using *in vivo* fluorescence spectroscopy with time resolution.

## Disclosures

All authors declare that there is no conflict of interests in this paper.

## Acknowledgements

The authors acknowledge the support of the Russian Science Foundation under project No. 21-15-00325. The authors appreciate the technical support and valuable discussions of Dr. Gerhard Holst (PCO AG, Kelheim, Germany).

## References

1. J. M. Llovet, R. K. Kelley, A. Villanueva, A. G. Singal, E. Pikarsky, S. Roayaie, R. Lencioni, K. Koike, J. Zucman-Rossi, and R. S. Finn, “[Hepatocellular carcinoma](#),” *Nature Reviews Disease Primers* 7(1), 6 (2021).
2. D. Mezale, I. Strumfă, A. Vanags, A. Kalva, D. Balodis, B. Strumfs, I. Fridrihsone, A. Abolins, and J. Gardovskis, “[Diagnostic Algorithm of Hepatocellular Carcinoma: Classics and Innovations in Radiology and Pathology](#),” Chapter 2 in *Hepatocellular Carcinoma-Advances in Diagnosis and Treatment*, C. T. Streba, C. C. Vere, and I. Rogoveanu, IntechOpen, UK, 2018.
3. M. M. Lukina, L. E. Shimolina, N. M. Kiselev, V. E. Zagainov, D. V. Komarov, E. V. Zagaynova, and M. V. Shirmanova, “[Interrogation of tumor metabolism in tissue samples ex vivo using fluorescence lifetime imaging of NAD \(P\) H](#),” *Methods and Applications in Fluorescence* 8(1), 14002 (2019).
4. K. Kandurova, V. Dremin, E. Zherebtsov, E. Potapova, A. Alyanov, A. Mamoshin, Y. Ivanov, A. Borsukov, and A. Dunaev, “[Fiber-Optic System for Intraoperative Study of Abdominal Organs during Minimally Invasive Surgical Interventions](#),” *Applied Sciences* 9(2), 217 (2019).
5. V. Dremin, E. Potapova, E. Zherebtsov, K. Kandurova, V. Shupletsov, A. Alekseyev, A. Mamoshin, and A. Dunaev, “[Optical percutaneous needle biopsy of the liver: A pilot animal and clinical study](#),” *Scientific Reports* 10(1), 14200 (2020).
6. E. Zherebtsov, M. Zajnulina, K. Kandurova, E. Potapova, V. Dremin, A. Mamoshin, S. Sokolovski, A. Dunaev, and E. U. Rafailov, “[Machine Learning Aided Photonic Diagnostic System for Minimally Invasive Optically Guided Surgery in the Hepatoduodenal Area](#),” *Diagnostics* 10(11), 873 (2020).
7. E. A. Zherebtsov, E. V. Potapova, A. V. Mamoshin, V. V. Shupletsov, K. Y. Kandurova, V. V. Dremin, A. Y. Abramov, and A. V. Dunaev, “[Fluorescence lifetime needle optical biopsy discriminates hepatocellular carcinoma](#),” *Biomedical Optics Express* 13(2), 633–646 (2022).
8. L. Kou, X. Jiang, H. Huang, X. Lin, Y. Zhang, Q. Yao, and R. Chen, “[The role of transporters in cancer redox homeostasis and cross-talk with nanomedicines](#),” *Asian Journal of Pharmaceutical Sciences* 15(2), 145–157 (2020).
9. T. S. Blacker, M. R. Duchon, “[Investigating mitochondrial redox state using NADH and NADPH autofluorescence](#),” *Free Radical Biology and Medicine* 100, 53–65 (2016).
10. K. Suhling, P. M. W. French, and D. Phillips, “[Time-resolved fluorescence microscopy](#),” *Photochemical & Photobiological Sciences* 4(1), 13–22 (2005).
11. M. T. Erkkilä, B. Bauer, N. Hecker-Denschlag, M. J. M. Medina, R. A. Leitgeb, A. Unterhuber, J. Gesperger, T. Roetzer, C. Hauger, W. Drexler, G. Widhalm, and M. Andreana, “[Widefield fluorescence lifetime imaging of protoporphyrin IX for fluorescence-guided neurosurgery: An ex vivo feasibility study](#),” *Journal of Biophotonics* 12(6), e201800378 (2019).
12. N. L. Lazarevich, O. A. Cheremnova, E. V. Varga, D. A. Ovchinnikov, E. I. Kudrjavitseva, O. V. Morozova, D. I. Fleishman, N. V. Engelhardt, and S. A. Duncan, “[Progression of HCC in mice is associated with a downregulation in the expression of hepatocyte nuclear factors](#),” *Hepatology* 39(4), 1038–1047 (2004).
13. E. Köhler, H.-J. Barrach, and D. Neubert, “[Inhibition of NADP dependent oxidoreductases by the 6-aminonicotinamide analogue of NADP](#),” *FEBS Letters* 6(3), 225–228 (1970).
14. I. J. Bickis, J. H. Quastel, “[Effects of metabolic inhibitors on energy metabolism of Ehrlich ascites carcinoma cells](#),” *Nature* 205(4966), 44–46 (1965).
15. H. Terada, “[Uncouplers of oxidative phosphorylation](#),” *Environmental Health Perspectives* 87, 213–218 (1990).
16. G. Palmer, D. J. Horgan, H. Tisdale, T. P. Singer, and H. Beinert, “[Studies on the respiratory chain-linked reduced nicotinamide adenine dinucleotide dehydrogenase: XIV. Location of the sites of inhibition of rotenone, barbiturates, and piericidin by means of electron paramagnetic resonance spectroscopy](#),” *Journal of Biological Chemistry* 243(4), 844–847 (1968).
17. F. Bartolomé, A. Y. Abramov, “[Measurement of Mitochondrial NADH and FAD Autofluorescence in Live Cells](#),” in *Mitochondrial Medicine*, Human Press, New York, 263–270 (2015).
18. M. A. Digman, V. R. Caiolfa, M. Zamai, and E. Gratton, “[The phasor approach to fluorescence lifetime imaging analysis](#),” *Biophysical Journal* 94(2), L14–L16 (2008).
19. C. Stringari, A. Cinquin, O. Cinquin, M. A. Digman, P. J. Donovan, and E. Gratton, “[Phasor approach to fluorescence lifetime microscopy distinguishes different metabolic states of germ cells in a live tissue](#),” *Proceedings of the National Academy of Sciences* 108(33), 13582–13587 (2011).
20. M. Y. Berezin, S. Achilefu, “[Fluorescence lifetime measurements and biological imaging](#),” *Chemical Reviews* 110(5), 2641–2684 (2010).
21. B. Chance, B. Schoener, R. Oshino, F. Itshak, and Y. Nakase, “[Oxidation-reduction ratio studies of mitochondria in freeze-trapped samples. NADH and flavoprotein fluorescence signals](#),” *Journal of Biological Chemistry* 254(11), 4764–4771 (1979).
22. D. K. Bird, L. Yan, K. M. Vrotsos, K. W. Eliceiri, E. M. Vaughan, P. J. Keely, J. G. White, and N. Ramanujam, “[Metabolic mapping of MCF10A human breast cells via multiphoton fluorescence lifetime imaging of the coenzyme NADH](#),” *Cancer Research* 65(19), 8766–8773 (2005).

23. H. Wang, X. Liang, Y. H. Mohammed, J. A. Thomas, K. R. Bridle, C. A. Thorling, J. E. Grice, Z. P. Xu, X. Liu, and D. H. G. Crawford, “[Real-time histology in liver disease using multiphoton microscopy with fluorescence lifetime imaging](#),” *Biomedical Optics Express* 6(3), 780–792 (2015).
24. S. Rodimova, D. Kuznetsova, N. Bobrov, V. Elagin, V. Shcheslavskiy, V. Zagainov, and E. Zagaynova, “[Mapping metabolism of liver tissue using two-photon FLIM](#),” *Biomedical Optics Express* 11(8), 4458–4470 (2020).
25. S. Elumalai, S. Managó, and A. C. De Luca, “[Raman Microscopy: Progress in Research on Cancer Cell Sensing](#),” *Sensors* 20(19), 5525 (2020).
26. L. Becker, N. Janssen, S. L. Layland, T. E. Mürdter, A. T. Nies, K. Schenke-Layland, and J. Marzi, “[Raman Imaging and Fluorescence Lifetime Imaging Microscopy for Diagnosis of Cancer State and Metabolic Monitoring](#),” *Cancers* 13(22), 5682 (2021).
27. S. Z. Al-Sammarraie, L. A. Bratchenko, E. N. Typikova, P. A. Lebedev, V. P. Zakharov, and I. A. Bratchenko, “[Silver Nanoparticles-Based Substrate for Blood Serum Analysis under 785 nm Laser Excitation](#),” *Journal of Biomedical Photonics & Engineering* 10301 (2022).